

Subwavelength Focusing Beam and Superresolution Ultrasonic Imaging Using a Core-Shell Lens

J. P. Leão-Neto¹, G. S. Cardoso², A. S. Marques², M. A. B. Andrade³, J. C. Adamowski⁴,
T. Z. Pavan⁵, G. T. Silva⁶, and J. H. Lopes^{2,*}

¹*Campus Arapiraca/Unidade de Ensino Penedo, Universidade Federal de Alagoas, Penedo, Alagoas, 57200-000, Brazil*


²*Grupo de Física da Matéria Condensada, Núcleo de Ciências Exatas, Universidade Federal de Alagoas, Arapiraca, AL 57309-005, Brazil*

³*Institute of Physics, University of São Paulo, São Paulo, São Paulo 05508-090, Brazil*

⁴*Department of Mechatronics and Mechanical Systems Engineering, University of São Paulo, São Paulo, São Paulo 05508-030, Brazil*

⁵*Department of Physics, University of São Paulo, Ribeirão Preto 14040-901, Brazil*

⁶*Physical Acoustics Group, Instituto de Física, Universidade Federal de Alagoas, Maceió, AL 57072-970, Brazil*

 (Received 16 October 2019; revised manuscript received 5 December 2019; published 30 January 2020)

The ability to manipulate acoustic fields beyond the diffraction limit offers possibilities for many applications, including ultrasound imaging and nondestructive testing. We numerically and experimentally report a simple method for subwavelength ultrasound focusing and superresolution imaging (i.e., images produced with a subwavelength spatial resolution) using a core-shell shaped lens. By changing the mechanical properties and size conditions of the lenses, we can significantly enhance the subwavelength properties of the focusing beams. These properties have a major effect on the image quality of ultrasonic systems. Using a carbon steel core and a Rexolite shell of total diameter of 12.8 mm positioned at a 2 MHz ($\lambda = 0.74$ mm) plane wave incident field, we show that a beam with intensity gain of 20 dB, full width at half maximum (FWHM) of 0.44 mm (0.6λ), and full length at half maximum (FLHM) of 2.74 mm (3.7λ) can be achieved. Moreover, we experimentally demonstrate that a superresolution imaging system using the core-shell lens can scan objects with subdiffraction information. The results show that the superresolution method can double the spatial resolution and the focal depth can be increased using an appropriate size of lens. The proposed design system can be easily applied to assisted superresolution acoustic microscopy devices.

DOI: [10.1103/PhysRevApplied.13.014062](https://doi.org/10.1103/PhysRevApplied.13.014062)

I. INTRODUCTION

Focusing acoustic fields in a subwavelength region has been a subject of considerable interest for research in many applications, from nondestructive testing [1] to medical diagnostic techniques [2]. However, the spatial resolution of conventional imaging systems is naturally limited by the wavelength of the incident field (diffraction limit) [3]. Many efforts have been made to develop new techniques to overcome the diffraction limit, including phononic crystals [4–6], nonlinear mixing [7–9], metamaterial lenses [10–18], nonlinear harmonic generation [19], and time-reversal mirrors [20,21]. Unfortunately, most of these techniques need a complex metamaterial engineering to manufacture the superlens or require extensive signal processing, which are difficult and expensive for practical applications. For these reasons, it is extremely important

to find new effective, inexpensive, and reliable methods to improve acoustic systems that overcome the limit imposed by diffraction.

Alternative methods using spherical shaped lenses have been used to overcome the difficulties encountered in manufacturing and in applying focusing systems beyond the diffraction limit. Focusing effects using a spherical balloon lens filled with carbon dioxide were demonstrated numerically, analytically, and experimentally [22,23]. In an analogy to optical photonic jet [24], numerical [25,26], and experimental [27,28] studies have shown that subwavelength ultrasound focusing beams (acoustic jet) can be achieved by using cylindrical and spherical objects with a radius of some wavelengths. Recently, a liquid-liquid core-shell lens was used to focus on an acoustic field with a spot narrower than 0.85λ [29]. Our work shares some similarities with the cited paper [29]. The main difference between them is that our work uses a fixed concentric core-shell lens, whereas [29] employs a

*jose.andrade@arapiraca.ufal.br

liquid-filled spherical container as the lens. The lens can be arranged with liquid layers along its diameter. A clear advantage of [29] is the possibility to change liquid region and, thus, the beam properties, whereas in our work the lens is fixed. On the other hand, the achieved resolution of our method is narrower than that in Ref. [29] (0.5λ versus 0.87λ) with a 20 dB gain. Taking into consideration the simplicity and its potential use in superresolution imaging systems, a more detailed analysis of the subwavelength acoustic beams is necessary.

Here, the ability of core-shell objects, such as a lens, to generate subwavelength focused acoustic beams is presented. The design and experimental demonstration of a simple and effective superresolution ultrasound imaging system using these beams are reported. The spatial resolution and focal depth of our system is numerically and experimentally measured computing the full width at half maximum (FWHM) and the full length at half maximum (FLHM) of the subwavelength beams. Furthermore, we show that the depth of field can be increased changing the core-shell size of the lens. A good signal-to-noise relationship is achieved owing the intensity gain produced by the lens. Two different lens sizes, composed of a carbon steel core and Rexolite shell, are used in this work. The capability and efficiency of our high-spatial-resolution imaging system are demonstrated by scanning a coin and a tissue-mimicking phantom sample containing subdiffraction features.

II. METHODS AND MATERIALS

The ability to generate focused acoustic fields in the subwavelength range using homogeneous spheres such as lenses has opened new possibilities to overcome the

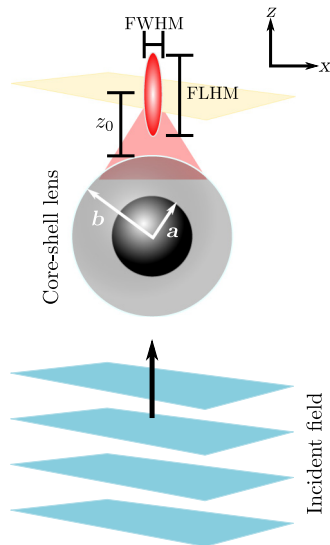


FIG. 1. Schematic configuration of the subwavelength ultrasound focusing beam generation using core-shell shaped lens.

TABLE I. Physical parameters of the core-shell lenses suspended in water at 20°C temperature.

Description	Value
Medium: Water [[30], p. 142]	
Density (ρ_0)	998 kg m ⁻³
Longitudinal velocity (c_0)	1480 ms ⁻¹
Core-shell lens size	
Lens 1:	
Radius (a)	3 mm
Radius (b)	6.4 mm
Ratio (a/b)	0.46
Lens 2:	
Radius (a)	6.35 mm
Radius (b)	13.45 mm
Ratio (a/b)	0.46
Core-shell lens acoustical parameters	
Core: Carbon steel	
Density (ρ_1)	7850 kg m ⁻³
Longitudinal velocity (c_{L1})	5900 ms ⁻¹
Shear velocity (c_{S1})	3230 ms ⁻¹
Shell: Rexolite [31]	
Density (ρ_2)	1060 kg m ⁻³
Longitudinal velocity (c_{L2})	2330 ms ⁻¹
Shear velocity (c_{S2})	1155 ms ⁻¹
Longitudinal absorption coefficient (α_L)	0.0028
Shear absorption coefficient (α_S)	0.0037
Fixing layer: Araldite XAW 1465	
Layer	0.05 mm
Density (ρ_2)	1060 kg m ⁻³
Longitudinal velocity (c_{L2})	1950 ms ⁻¹
Shear velocity (c_{S2})	1480 ms ⁻¹

diffraction limit in recent years [27]. The beam arises in the near field of the ball-lens shadow side. Here, these beams features are enhanced and manipulated using homemade core-shell objects operating as acoustic lenses. Figure 1 schematically shows the subwavelength focusing phenomenon of the core-shell lens when irradiated by an incident acoustic field. The internal and external radii of the core-shell lens are denoted by a and b , respectively. The core and shell are fixed by a thin Araldite layer. Two different sizes of lens, namely lens 1 and 2, are used in this work. The physical parameters and sizes of the lenses are presented in Table I. The lens is located at the origin of the coordinate system and the incident wave is generated by a circular transducer. The acoustic field arriving at the core-shell lens is focused into a small spot, the center of which is located at a working distance z_0 from the lens rear surface (see Fig. 1). In this paper, the working distance is defined from the center of the core-shell lens to the peak intensity position at the focus.

A. Numerical model

Finite-element methods (FEM) through COMSOL MULTIPHYSICS software is used to simulate the subwavelength

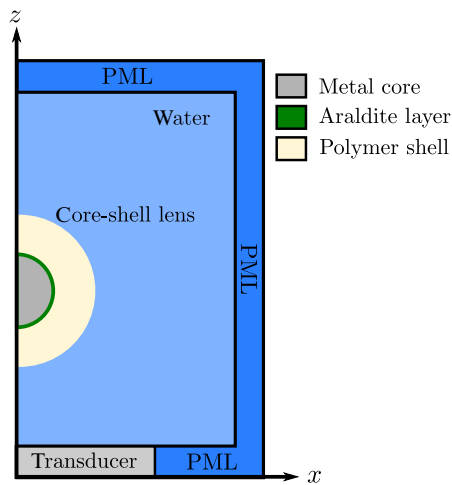


FIG. 2. Schematic diagram of the two-dimensional axisymmetric simulation geometry for subwavelength acoustic beam generation using a finite-element method in COMSOL. All simulations are performed with one wavelength of PML layer.

focusing beam generation by a core-shell shaped lens immersed in water. Pressure acoustics and solid mechanics modules are used to describe the medium and lens domain, respectively. Owing to the symmetry of our problem, a two-dimensional axisymmetric geometry model is implemented Fig. 2. Three concentric semicircles are designed to represent the metal core, Araldite fixing layer, and polymer shell, respectively. The fixing layer is used for bonding the core to the shell. A rectangle geometry is drawn to model the transducer. The simulated subwavelength beams are obtained by computing the first-order acoustic pressure on the shadow side of the lens. Parametric simulations modifying the core-shell ratio dependence are carefully conducted to find the optimal subwavelength beam conditions. Both frequency domain (plane wave incidence) and transient (single pulse) studies are analyzed. For all

the simulations, perfect matched layers (PMLs) are added to the right, bottom, and top boundaries of the model to eliminate boundary-reflected acoustic waves. For proper calculations, it is essential to use the appropriate number of mesh elements. A convergence analysis is carried out and the mesh element size is set to be $1/15$ of the incident wavelength. All simulations are carried out in a desktop with an AMD Ryzen 3.2 GHz, 64-bit processor and 64 GB RAM with a WINDOWS operating system.

B. Experimental setup

Figure 3 shows the setup configuration used for the subwavelength focusing beam generation. First, a single-element ultrasound flat transducer (Model V305-SU, Panametrics 2.25 MHz) with a circular radiating face of 19 mm in diameter is driven by a signal generator (Model 33250A, Agilent Technologies USA) and subsequently amplified by an amplifier (Model 150A, Amplifier Research Corp., Souderton, PA) with a 2 MHz tone burst of 40 cycles. The core-shell lens is positioned 560 mm away from the transducer face to guarantee that a plane wave front reaches at the lens surface. After scattering, the acoustic pressure is measured on the shadow side of the core-shell lens by a calibrated needle hydrophone (Model HP series, Precision Acoustics, Dorchester, UK) with a diameter of $200\mu\text{m}$. The hydrophone is attached to a motorized mechanism for scanning over the xz plane ($10\text{ mm} \times 10\text{ mm}$) with a spatial resolution of $50\mu\text{m}$. The entire experimental setup is immersed in a $1500\text{ mm} \times 600\text{ mm} \times 600\text{ mm}$ water tank at 20°C temperature. The acoustic signal is collected by an acquisition system and postprocessed using MATLAB R2018a software (Mathworks, Natick, MA, USA).

To experimentally demonstrate the superresolution ability of our system, images of sample objects are produced using the pulse-echo technique. A short pulse is generated with a pulse-receiver (Model 5077PR square-wave OLYMPUS, USA), excitation voltage 100 V. The lens is

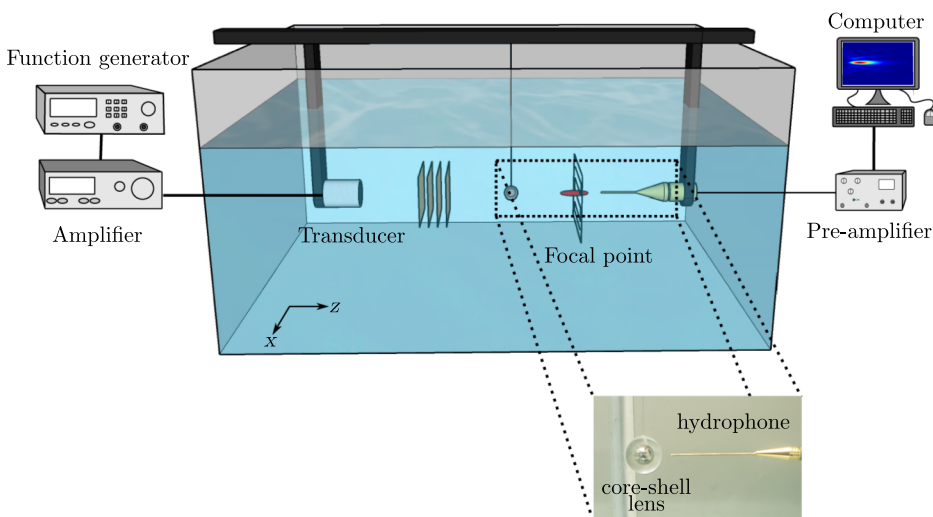


FIG. 3. Subwavelength ultrasound focused beam setup.

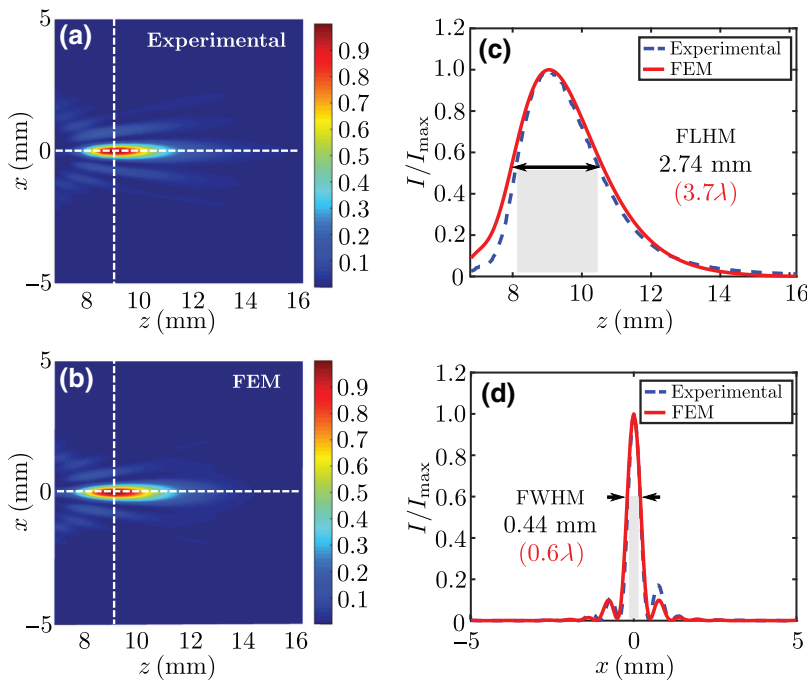


FIG. 4. Acoustic subwavelength focused beam produced by the core-shell lens 1 scattered by a continuous incident plane wave. The position of maximum intensity characterizes the main features of the subwavelength focused beam. (a) Experimental and (b) numerical normalized intensity (I/I_{\max}) profiles along the z direction. The distance between the incident field and the core-shell lens is 570 mm and the beam focus is located at $z = 8.8$ mm from the origin of coordinate system. (c) Axial intensity plots ($z > a$) and (d) transverse intensity plots at ($z = 9.05$ mm) of the FEM, red solid line, with experimental data, dashed blue lines. All the intensities are normalized to the peak intensity computed by the FEM ($I/I_0 = 87$).

fixed by three strands of hair (with 120° between them). The strands are glued to a 12 cm (350λ) ring and positioned 50 mm from the transducer surface. We thus may expect that the support will not interfere with the image formation process. After reaching the core-shell lens, the pulsed ultrasonic beam is focused at a working distance z_0 in the shadow side of the lens. Therefore, the imaging plane of our system is located at the focal spot in the shadow side of the lens. The sample to be imaged is fixed in a motorized scanning system and translated in the imaging plane with steps of $50\ \mu\text{m}$. The scattered wave in the imaging plane regions is refocused by the lens, collected by the transducer and postprocessed using the software MATLAB 2015R to create the final C-mode image.

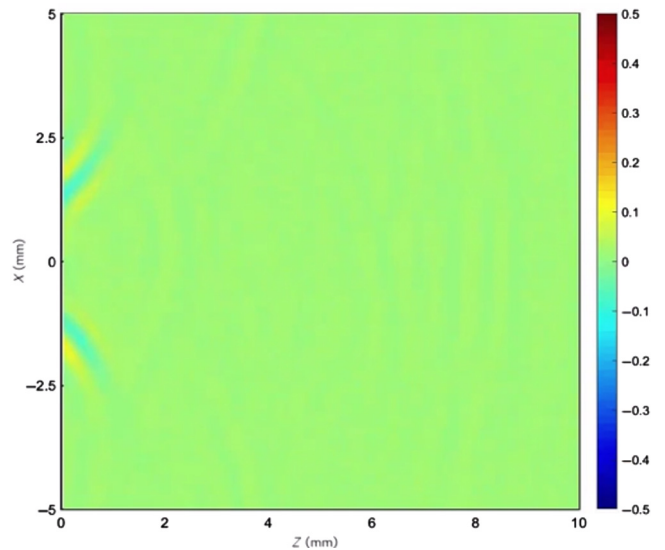
III. RESULTS AND DISCUSSION

A. Subwavelength focused beam generation: plane wave excitation

First, the ability of the core-shell lens to generate a subwavelength focused beam is analyzed using a 2 MHz plane wave incident acoustic field. Numerical simulations and experimental analyses are conducted using a homemade carbon-steel core and Rexolite shell with inner and outer radius of $a = 3$ mm and $b = 6.4$ mm, respectively. The core and shell are fixed by a 0.05 mm Araldite layer. The acoustic pressure field behind the lens ($z = z_0$) is collected using a 0.2 mm calibrated needle hydrophone. The origin of the coordinate system is placed in the center of the lens. For this configuration, a subwavelength focusing beam with $\text{FWHM} = 0.6\lambda$, $\text{FLHM} = 3.7\lambda$, and intensity gain of 20.2 dB is achieved. The beam had a working distance of

$z_0 = 8.8\lambda$. These properties should play an effective role in superresolution imaging systems.

Comparative results between numerical and experimental analyses using the core-shell lens 1 and a continuous acoustic field are presented in Fig. 4. Figures 4(a) and 4(b) show the normalized intensity along the z -direction obtained by FEM and experimental data, respectively. To guarantee an incident plane wave excitation, the lens is positioned 560 mm away from transducer. The horizontal and vertical dashed white lines are positioned in the



VIDEO 1. Propagation of a superfocused ultrasound pulse measured at the experimental superfocused ultrasound pulse propagation at the shadow region of the core-shell lens in water.

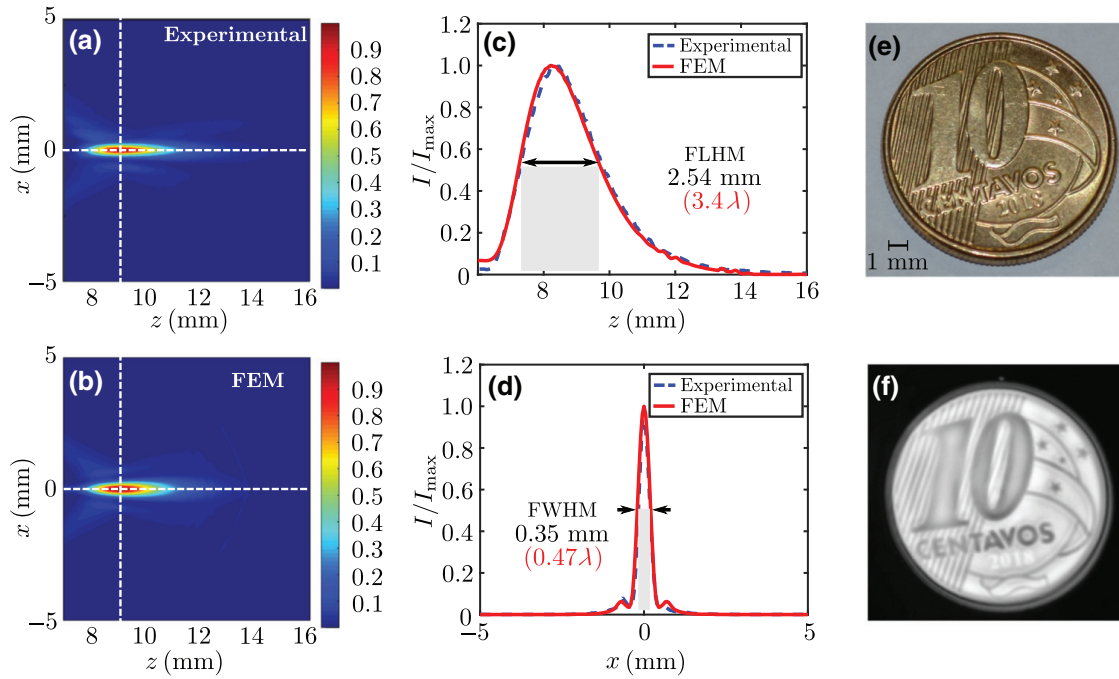


FIG. 5. Pulse-echo superresolution imaging results. (a) Experimental and (b) FEM normalized intensity profile generated by a core-shell (lens 1) placed 50 mm away from a flat transducer pulse-echo system. The position of maximum intensity ($z = 9.05$ mm) is considered the image plane. (c) Experimental (blue dashed line) and FEM (red solid line) normalized intensity distribution along the axial direction z . (d) Experimental (blue dashed line) and FEM (red solid line) normalized intensity distribution along the transverse direction at the maximum intensity point. A working distance of 2.4 mm is found for this configuration. (e) Image of a 10 cents Brazilian coin sample used in this superresolution experiment. The sample is positioned specifically at the beam focus. (f) Measured image obtained by recording the peak-to-peak acoustic pressure amplitude in a 22×22 mm xy plane.

axial and transverse direction, respectively. In Fig. 4(c), the axial intensity of FEM (solid red line) and experimental measurement (dashed blue line) are shown, starting at position 6.4 mm located on the shadow surface of the core-shell lens. The peak intensity is located at 9.05 mm. Figure 4(d) shows the intensity distribution along the transverse plane, at the focal point for both the numerical and experimental studies. All the results are normalized by the FEM maximum intensity value (I_{\max}), $I_{\max}^{\text{FEM}} = 87$. An excellent agreement is obtained between the FEM and experimental results. We show the video animation (Video 1) of an experimentally measured ultrasound pulse in the lens focal region $z > b$. We see that the superfocused beam is a propagating and not an evanescent wave.

B. Superresolution imaging system

To demonstrate the viability of a superresolution ultrasound imaging system using subwavelength beams produced by core-shell-like lens, a similar experimental setup is used; see Fig. 3. The setup mainly consists of three parts: (1) an ultrasound generation system, (2) a core-shell lens, and (3) an object fixed in a motorized control system. A short pulse of wavelength 0.74 mm is generated and scattered by a core-shell lens placed 50 mm from the transducer surface. Reflected echoes from the sample

are refocused by the lens and recorded for future postprocessing. Subwavelength ultrasonic C-mode images of two objects using both lens 1 and lens 2 are demonstrated.

1. Spatial resolution

Prior to showing the experimentally measured superresolution imaging results, we demonstrate the subwavelength focusing effect on an incident pulsed signal. A similar approach is used to compute the descriptive parameters of the beam. Figures 5(a) and 5(b) show the experimental data and numerical simulation, respectively, of the acoustic peak intensity profile of the focused beam generated by core-shell lens 1. The horizontal and vertical white dashed lines represent the axial and transverse lines used to plot one-dimensional results. Figures 5(c) and 5(d) present the axial and transverse intensity plots, respectively. Our results show that a subwavelength focused beam with $\text{FWHM} = 0.35$ mm (0.48λ), $\text{FLHM} = 2.54$ mm (3.39λ), and 2.45 mm work distance is achieved. According to the Rayleigh criterion [3], the quality of the spatial resolution is related to the FWHM. In addition, the intensity gain plays an important role in the signal noise relation of the image. Therefore, this beam has great potential for applications in the superresolution imaging system.

To experimentally show the superresolution imaging from our system, a Brazilian 10-cent coin of 20 mm diameter containing subdiffraction geometrical features on its face is used. Figure 5(e) shows a photograph of the coin. The pulse signal produced by the ultrasonic system is focused on the shadow size of the lens at a working distance $z_0 = 2.45$ mm (3.31λ). This is the depth adopted to obtain the C-mode image for this configuration. A three-dimensional motorized scanning system is programmed to scan the sample on a 22×22 mm² xy image plane with steps of 0.05 mm. At each x - y position, echoes from the object are refocused by the lens and collected by the transducer and postprocessed to generate the final image. The experimental superresolution image of our system is shown in Fig. 5(f). The coin surface presents some parallel lines that are spaced by a distance of 350 μ m. The spacing between these lines is measured using an optical microscope. This distance corresponds to nearly half wavelength. The lines are well-resolved by our superresolution method, as illustrated in the ultrasound image in Fig. 5(f).

2. Penetration depth phantom image

The capacity of changing the beam features using different core-shell sizes is experimentally presented by

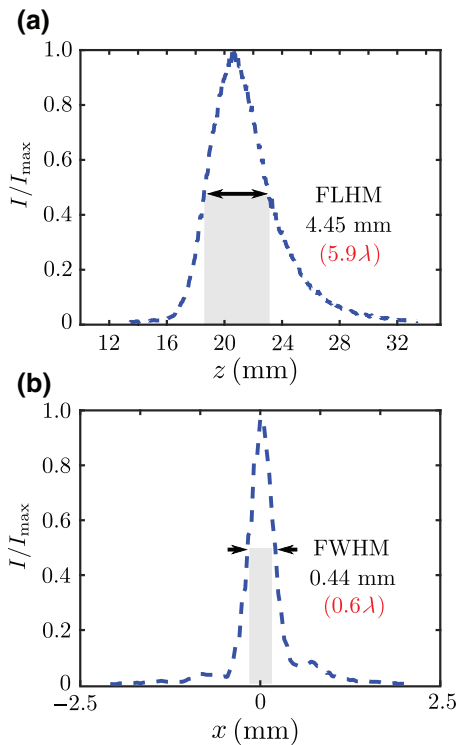


FIG. 6. Subwavelength beam features generated by core-shell lens 2 in a 2 MHz pulsed ultrasound field. The working distance obtained by this lens is $z_0 = 8.4$ mm. (a) Axial intensity distribution with $z > (a + b)$. (b) The intensity along the transverse direction at $z = 21.85$.

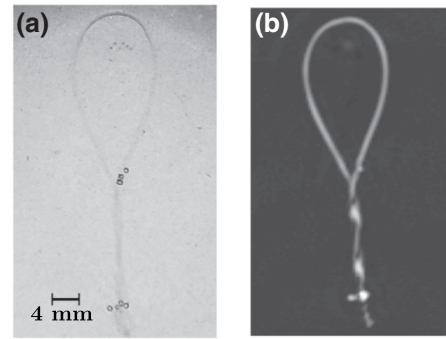


FIG. 7. Superresolution image obtained of a phantom with a knotted thread positioned at 6 mm from the surface. (a) Photograph of the phantom sample. (b) Image generated by the superresolution core-shell system.

imaging a phantom sample. The tissue-mimicking phantom is manufactured using a copolymer styrene-ethylene and/or butylene-styrene (SEBS; Kraton G 1650 M, Kraton Polymers, Paulinia, SP, Brazil) in mineral oil gel. This is a translucent gel presenting acoustic and elastic properties similar to tissue [32,33]. The gel is prepared using the SEBS polymer at a dry weight concentration of 15% following the procedure described in [32]. The final phantom had a cylindrical shape with diameter 50 mm and height 25 mm. Polyvinyl chloride microparticles, of mean diameter 40 μ m (Solvin SA), are added at a 1% dry weight concentration to serve as acoustic wave scatterers.

The phantom contains a 400 μ m transparent nylon thread arranged in a knot shape. The knot is placed 6 mm away from the phantom surface. Owing to the depth of field limitation of lens 1 (2.45 mm), a second lens (lens 2) is built to obtain a deeper focus. Figure 6(a) shows the axial normalized intensity along the z axis of the focused field generated by lens 2. A working distance $z_0 = 21.85$ mm and a FLHM = 4.45 mm are achieved. The intensity field distribution along the transverse direction $z = 21.85$ mm is illustrated in Fig. 6(b). For this lens configuration the spatial resolution obtained computing the FWHM is 0.44 mm. Figure 7(a) shows a photograph of the phantom sample. Figure 7(b) presents the superresolution image obtained with the phantom. All the parts of the knot inside the phantom are clearly visible.

IV. SUMMARY AND CONCLUSION

In conclusion, we have numerically and experimentally demonstrated that subwavelength focused beams can be produced by core-shell shaped lens in a low-megahertz-frequency regime. We have found that by changing the core-shell ratio, the focusing beam features can be enhanced. Shaping acoustic fields is a crucial way to achieve superresolution ultrasound imaging. We also demonstrate that a superresolution system can be designed

using these lens by scanning a coin and a phantom structure containing subdiffraction details. Excellent agreement between simulations and experimental data is achieved. Given the design simplicity and efficiency, our work may have a major effect on the new subwavelength acoustic devices that can be readily adapted to ultrasound imaging systems, as well as acoustic microscopy technology.

ACKNOWLEDGMENTS

This work was partially supported by the Brazilian agencies Conselho Nacional de Desenvolvimento Científico e Tecnológico-CNPq (Grants No. 309375/2018-5 and No. 437757/2018-8) and Fundação de Amparo à Pesquisa do Estado de Alagoas-FAPEAL (Grant No. 1024/2016).

-
- [1] A. Webb and G. C. Kagadis, Introduction to biomedical imaging, *Med. Phys.* **30**, 2267 (2003).
- [2] J. Blitz and G. Simpson, *Ultrasonic Methods of Non-destructive Testing*, edited by Netherlands Springer (Springer, London, UK, 1995), Vol. 2.
- [3] L. R. Rayleigh, Investigations in optics, with special reference to the spectroscope, *London, Edinburgh, Dublin Philos. Mag. J. Sci* **8**, 261 (1879).
- [4] S. Yang, J. H. Page, Z. Liu, M. L. Cowan, C. T. Chan, and P. Sheng, Focusing of Sound in a 3D Phononic Crystal, *Phys. Rev. Lett.* **93**, 024301 (2004).
- [5] A. Sukhovich, L. Jing, and J. H. Page, Negative refraction and focusing of ultrasound in two-dimensional phononic crystals, *Phys. Rev. B* **77**, 014301 (2008).
- [6] J. F. Robillard, J. Bucay, P. A. Deymier, A. Shelke, K. Muralidharan, B. Merheb, J. O. Vasseur, A. Sukhovich, and J. H. Page, Resolution limit of a phononic crystal superlens, *Phys. Rev. B* **83**, 224301 (2011).
- [7] M. Fatemi and J. F. Greenleaf, Ultrasound-stimulated vibro-acoustic spectrography, *Science* **280**, 82 (1998).
- [8] G. T. Silva, A. C. Frery, and M. Fatemi, Image formation in vibro-acoustography with depth-of-field effects, *Comput. Med. Imaging Graph.* **30**, 321 (2006).
- [9] A. L. Baggio, H. A. S. Kamimura, J. H. Lopes, A. A. O. Carneiro, and G. T. Silva, Parametric array signal in confocal vibro-acoustography, *Appl. Acoust.* **126**, 143 (2017).
- [10] Sébastien Guenneau, Alexander Movchan, Gunnar Pétursson, and S. Anantha Ramakrishna, Acoustic metamaterials for sound focusing and confinement, *New J. Phys.* **9**, 399 (2007).
- [11] Xianyu Ao and C. T. Chan, Far-field image magnification for acoustic waves using anisotropic acoustic metamaterials, *Phys. Rev. E* **77**, 025601 (2008).
- [12] S. Zhang, L. Yin, and N. Fang, Focusing Ultrasound with an Acoustic Metamaterial Network, *Phys. Rev. Lett.* **102**, 194301 (2009).
- [13] J. Li, L. Fok, X. Yin, G. Bartal, and X. Zhang, Experimental demonstration of an acoustic magnifying hyperlens, *Nat. Mater.* **8**, 931 (2009).
- [14] J. Zhu, J. Christensen, J. Jung, L. Martin-Moreno, X. Yin, L. Fok, X. Zhang, and F. J. Garcia-Vidal, A holey-structured metamaterial for acoustic deep-subwavelength imaging, *Nat. Commun.* **7**, 52 (2011).
- [15] Xiaoming Zhou, M. Badreddine Assouar, and Mourad Oudich, Subwavelength acoustic focusing by surface-wave-resonance enhanced transmission in doubly negative acoustic metamaterials, *J. Appl. Phys.* **116**, 194501 (2014).
- [16] Nadège Kaina, Fabrice Lemoult, Mathias Fink, and Geoffroy Lerosey, Negative refractive index and acoustic superlens from multiple scattering in single negative metamaterials, *Nat. Lett.* **525**, 77 (2015).
- [17] Jong Jin Park, Choon Mahn Park, K. J. B. Lee, and Sam H. Lee, Acoustic superlens using membrane-based metamaterial, *Appl. Phys. Lett.* **106**, 051901 (2015).
- [18] Tuo Liu, Fei Chen, Shanjun Liang, He Gao, and Jie Zhu, Subwavelength Sound Focusing and Imaging via Gradient Metasurface Enabled Spoof Surface Acoustic Wave Modulation, *Phys. Rev. Appl.* **11**, 034061 (2019).
- [19] D. Rugar, Resolution beyond the diffraction limit in the acoustic microscope: A nonlinear effect, *J. Appl. Phys.* **56**, 1338 (1984).
- [20] M. Fink, D. Cassereau, A. Derode, C. Prada, P. Roux, M. Tanter, J.-L. Thomas, and F. Wu, Time-reversed acoustics, *Rep. Prog. Phys.* **63**, 1933 (2000).
- [21] G. Lerosey, J. de Rosny, A. Tourin, and M. Fink, Focusing beyond the diffraction limit with far-field time reversal, *Science* **315**, 1120 (2007).
- [22] D. C. Thomas, K. L. Gee, and R. S. Turley, A balloon lens: Acoustic scattering from a penetrable sphere, *Am. J. Phys.* **77**, 197 (2009).
- [23] M. A. P. Borrero, M. Pérez-Saborid, and J. M. F. García, Acoustic scattering from a spherical lens irradiated by a finite transducer: Focusing effect and refraction, *Am. J. Phys.* **79**, 401 (2011).
- [24] Z. Chen and A. Taflove, Photonic nanojet enhancement of backscattering of light by nanoparticles: A potential novel visible-light ultramicroscopy technique, *Opt. Expr.* **12**, 1214 (2004).
- [25] J. H. Lopes, J. P. Leão-Neto, I. V. Minin, O. V. Minin, and G. T. Silva, in *Proceedings of the 2nd International Congress on Acoustics ICA 2016* (Buenos Aires, Argentina, 2016), pp. 1–7. www.ica2016.org.ar/ica2016proceedings/ica2016/ICA2016-0943.pdf.
- [26] O. V. Minin and I. V. Minin, Acoustojet: Acoustic analogue of photonic jet phenomenon based on penetrable 3d particle, *Opt. Quant. Electron.* **49**, 54 (2017).
- [27] J. H. Lopes, M. A. B. Andrade, J. P. Leão-Neto, J. C. Adamowski, I. V. Minin, and G. T. Silva, Focusing Acoustic Beams with a Ball-Shaped Lens Beyond the Diffraction Limit, *Phys. Rev. Applied* **8**, 024013 (2017).
- [28] Daniel Veira Canle, Tuukka Kekkonen, Joni Mäkinen, Tuomas Puranen, Heikki J. Nieminen and Antti Kuronen, Sami Franssila, Tapio Kotiaho, Ari Salmi, and Edward Hægström, Practical realization of a sub $\lambda/2$ acoustic jet, *Sci. Rep.* **9**, 5189 (2019).
- [29] Sergio Péez-López, Pilar Candelas, José Miguel Fuster, Constanza Rubio, Oleg V. Minin, and Igor V. Minin, Liquid-liquid core-shell configurable mesoscale spherical

- acoustic lens with subwavelength focusing, *Appl. Phys. Express* **12**, 087001 (2019).
- [30] D. R. Lide, ed., *CRC Handbook of Chemistry and Physics* (CRC Press, Boca Raton, FL, 2005), 85th ed.
- [31] C. Cadot, J.-F. Saillant, and B. Dulmet, in *Proceedings of the 19th World Conference on Non-Destructive Testing 2016* (Northampton, UK, 2016), pp. 1–9. <http://ndt.net/?id=19542>.
- [32] L. C. Cabrelli, P. I. Pelissari, A. M. Deana, A. A. Carneiro, and T. Z. Pavan, Stable phantom materials for ultrasound and optical imaging, *Phys. Med. Biol.* **62**, 432 (2017).
- [33] L. C. Cabrelli, F. W. Grillo, D. R. T. Sampaio, A. A. Carneiro, and T. Z. Pavan, Acoustic and elastic properties of glycerol in oil-based gel phantoms, *Ultrasound Med. Biol.* **43**, 2086 (2017).